J. Fluid Mech. (2001), *vol.* 428, *pp.* 107–131. Printed in the United Kingdom

The effect of convective heat transfer on unsteady boundary-layer separation

By K. W. CASSEL

Fluid Dynamics Research Center,
Mechanical, Materials and Aerospace Engineering Department,
Illinois Institute of Technology, Chicago, IL 60616, USA

(Received 16 April 1999 and in revised form 20 July 2000)

The unsteady evolution of a boundary layer induced by a rectilinear vortex convecting above a heated surface is considered numerically. This model problem is representative of the types of interactions that can occur when vortices encounter solid surfaces in a wide variety of diverse applications involving high-Reynolds-number and high-Grashof-number flows. It is known that in the case without heat transfer, the vortex-induced boundary layer evolves toward a singularity as it forms a sharp spike that erupts away from the surface. Numerical solutions of the unsteady mixed-convection boundary-layer equations in the Boussinesq limit are obtained in Lagrangian coordinates. Solutions for various values of the inclination angle of the surface and Grashof number show that the coupling between the fluid flow and heat transfer can have a dramatic effect upon the transport of momentum and energy within the boundary layer induced by the vortex. The unsteady eruption convects high-temperature, near-wall fluid away from the surface and causes large gradients in the thermal boundary layer. The buoyancy force acting on the heated boundary-layer fluid can also have a significant impact on the unsteady separation process, either accelerating or delaying it, depending upon the inclination angle of the surface.

1. Introduction

Unsteady separation occurs in a wide variety of flows of practical interest; it occurs, for example, in dynamic stall of airfoils, juncture flows and turbulent boundary layers (see, for example, Doligalski, Smith & Walker 1994). The common feature in these diverse flow environments is an adverse pressure gradient imposed locally on the surface that causes a recirculation region to form within the boundary layer. Unsteady separation culminates in the local eruption of high-vorticity fluid from adjacent to the surface into the outer inviscid flow. Although these events occur very rapidly and on small spatial scales, they often alter the large-scale flow significantly and play a central role in the dynamics of the flows mentioned above; therefore, much attention has been given to providing a detailed physical explanation of the events leading up to and occurring during the unsteady separation process. For example, Van Dommelen & Shen (1982) and Peridier, Smith & Walker (1991*a*) have computed the unsteady boundary-layer equations for flows involving unsteady separation; Elliott, Cowley & Smith (1983), Smith (1988), Peridier, Smith & Walker (1991*b*) and Cassel, Smith & Walker (1996) have considered the influence of viscous–inviscid interaction on the unsteady separation process; Hoyle, Smith & Walker (1991) and Li *et al.* (1998) have investigated the effect of normal pressure gradients, and Cassel (1996, 2000) has

obtained numerical solutions of the full Navier–Stokes equations for a flow involving unsteady separation to corroborate these three stages.

While there is still much that is not understood about the unsteady separation process itself, there has been an increasing amount of work in recent years aimed at determining the influence of various mechanisms on the unsteady separation process. For example, it has been demonstrated by Degani, Walker & Smith (1998) that it is possible to suppress unsteady separation using a moving wall, and Modi, Munshi & Bandyopadhyay (1998) have shown that a moving wall at the leading edge of an airfoil can delay the angle of attack at which stall occurs. Similarly, Chandrasekhara, Wilder & Carr (1997) have demonstrated that the stall angle can be delayed using an adaptive airfoil leading edge that is capable of changing shape locally. Leading-edge suction has also been shown to be effective in controlling formation of the dynamic stall vortex on airfoils by Karim & Acharya (1994) and Alrefai & Acharya (1996). Finally, the effect of the interaction between a flexible surface and an external flow on unsteady separation has been investigated by Kiran, Varley & Walker (1996) and Pal & Sinha (1998).

One influence that has not been considered is that of convective heat transfer on the unsteady separation process. There are many applications, such as in gas turbines, where unsteady separation can occur in an environment where heat transfer is also an important consideration. Puhak, Degani & Walker (1995) have considered the unsteady separation that occurs upstream of obstacles. They obtained numerical solutions for the flow in the symmetry plane upstream of a circular cylinder mounted perpendicular to a surface and a two-dimensional ridge on a surface; in both cases the surface was maintained at a temperature different from the mainstream. It was shown that the development of an unsteady eruption leads to significant variations in the heat transfer rate from the surface. Their investigation only considered the forced-convection flow, in which the momentum equation is decoupled from the energy equation and the heat transfer does not influence the fluid flow.

Investigations of the effect of mixed convection, where the fluid flow and heat transfer are fully coupled, on boundary-layer separation have been limited to the steady case. Stewartson (1962) was the first to consider the influence of heat transfer on the boundary layer in the vicinity of a Goldstein (1948) singularity which occurs at a point of zero wall shear stress. He found that the singularity only occurs at a point of zero wall shear stress if the heat flux at that point is also zero. A modification to Stewartson's expansion near a point of zero wall shear has been provided by Buckmaster (1970) for the cold wall case. The flow past a semi-infinite vertical plate in which the buoyancy force opposes the boundary layer has been considered by Merkin (1969), who obtained a combination of series and numerical solutions up to separation for an isothermal surface, and Wilks (1974), who has considered the case with a constant surface heat flux. Both the isothermal and constant heat flux conditions have been studied by Hunt & Wilks (1980) for a vertical plate. Davies & Walker (1977) have also obtained numerical solutions for a flow involving a linearly retarded mainstream velocity and the boundary layer on a circular cylinder. The mechanism by which a singularity could occur upstream of the point of zero wall shear stress on a horizontal cold wall has been described by Schneider & Wasel (1985). More recent investigations have focused on the effect of the inclination angle of the plate (Wickern 1991*a*), the influence of the Prandtl number (Wickern 1991*b*), the form of the singularity on a horizontal insulated wall (Daniels 1992; Daniels & Gargaro 1993) and the separation due to a step change in surface temperature (Higuera 1997). The latter study involves a triple-deck structure centred at the location where the step change occurs.

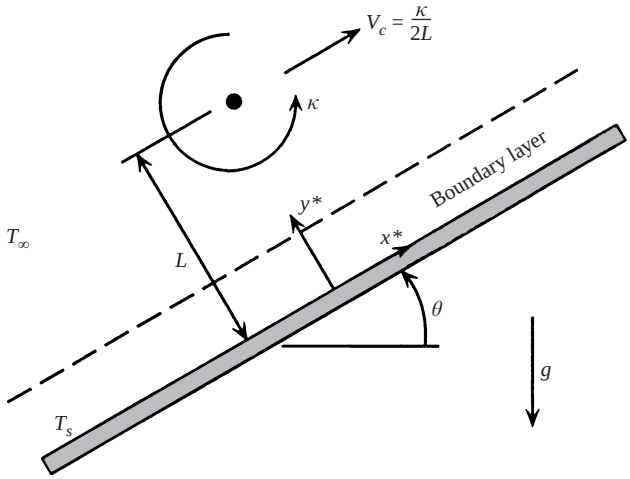

FIGURE 1. Schematic of the vortex-induced boundary layer.

The objective of the present investigation is to determine the effect of mixed convection on *unsteady* boundary-layer separation and the influence of the evolving boundary-layer flow on the convective heat transfer. In order to facilitate this, a model problem is considered involving a rectilinear vortex travelling in an otherwise stagnant fluid above an infinite plane wall that is heated to a temperature above that of the ambient fluid and is oriented at an arbitrary inclination angle. For the case without heat transfer (or with forced convection) the boundary-layer flow for this model problem is given by Peridier *et al.* (1991*a*). Here the coupled unsteady boundary-layer momentum and energy equations are formulated in the Boussinesq limit and solved numerically using the Lagrangian formulation. The results show that not only does unsteady separation have a dramatic influence upon the convective heat transfer, but mixed convection can also have a significant effect upon the unsteady separation process. In particular, it is found that, depending upon the orientation of the surface, unsteady separation can either be accelerated or delayed by the action of the buoyancy force.

2. Vortex-induced mixed-convection boundary layer

Consider a rectilinear vortex of strength κ located in an otherwise stagnant fluid and a distance L above an infinite plane surface as shown schematically in figure 1. The surface is inclined an angle θ from the horizontal and heated to a temperature T_s, which is above the ambient fluid temperature T_∞. The dimensional streamwise and normal coordinates (x^*, y^*) are defined along the surface and normal to the surface, respectively, and velocity components (u^*, v^*) are defined in the (x^*, y^*) coordinate directions. From inviscid theory (Walker 1978), a vortex with positive rotation remains a distance L above the wall and is convected to the right with constant velocity $V_c = \kappa/2L$ by its image below the surface. The characteristic length L, vortex speed V_c and time scale L/V_c are used to define dimensionless variables, and the problem is formulated in a frame of reference moving with the vortex. In this frame the vortex is centred at $x = 0$ and the wall moves in the negative x-direction, with dimensionless velocity $u_w = -1$. Due to the inviscid slip velocity induced by the vortex on the surface, a boundary layer of thickness $O(Re^{-1/2})$ forms across which the velocity

is adjusted to relative rest at the surface. The Reynolds number is defined here as $Re = LV_c/v = \kappa/2v$, where v is the kinematic viscosity. Walker (1978) shows that the dimensionless mainstream velocity at the outer edge of the boundary layer for this problem is

$$U_\infty(x) = -1 + \frac{4}{x^2+1}. \tag{2.1}$$

The corresponding pressure distribution, $\partial p/\partial x = -U_\infty \, \mathrm{d}U_\infty/\mathrm{d}x$, indicates that there is a region of adverse pressure gradient acting on the boundary layer between the vortex centre at $x = 0$ and the inviscid stagnation point located at $x = \sqrt{3}$.

2.1. *Eulerian formulation*

For two-dimensional laminar flow in the Boussinesq approximation, with the transport coefficients being assumed constant, the boundary-layer equations for mixed convection over a flat surface at arbitrary angle of inclination θ from the horizontal are given in dimensional form by

$$\frac{\partial u^*}{\partial t^*} + u^*\frac{\partial u^*}{\partial x^*} + v^*\frac{\partial u^*}{\partial y^*} = -\frac{1}{\rho}\frac{\partial p^*}{\partial x^*} + v\frac{\partial^2 u^*}{\partial y^{*2}} + g\beta\sin\theta(T^* - T_\infty), \tag{2.2a}$$

$$0 = -\frac{1}{\rho}\frac{\partial p^*}{\partial y^*} + g\beta\cos\theta(T^* - T_\infty), \tag{2.2b}$$

$$\frac{\partial T^*}{\partial t^*} + u^*\frac{\partial T^*}{\partial x^*} + v^*\frac{\partial T^*}{\partial y^*} = \alpha\frac{\partial^2 T^*}{\partial y^{*2}}, \tag{2.2c}$$

$$\frac{\partial u^*}{\partial x^*} + \frac{\partial v^*}{\partial y^*} = 0. \tag{2.2d}$$

Here ρ is density, v is kinematic viscosity, g is the acceleration constant, β is the coefficient of thermal expansion, α is the thermal diffusivity, p^* is the pressure and T^* is the temperature. In a frame of reference moving with the vortex, the boundary conditions are

$$u^* = -V_c, \quad v^* = 0, \quad T^* = T_s \qquad \text{at } y^* = 0, \tag{2.3a}$$

$$u^* \to V_c U_\infty(x^*), \quad T^* \to T_\infty \qquad \text{as } y^* \to \delta, \tag{2.3b}$$

where δ is the outer edge of the boundary layer. The boundary layer has a thickness of $O(Re^{-1/2})$; therefore, dimensionless boundary-layer variables are defined as follows:

$$x = \frac{x^*}{L}, \quad y = \frac{y^*}{L}Re^{1/2}, \quad t = \frac{t^* V_c}{L}, \tag{2.4a}$$

$$u = \frac{u^*}{V_c}, \quad v = \frac{v^*}{V_c}Re^{1/2}, \quad p = \frac{p^*}{\rho V_c^2}, \quad T = \frac{T^* - T_\infty}{T_s - T_\infty}. \tag{2.4b}$$

Substituting these variables into the boundary-layer equations (2.2) gives

$$\frac{\partial u}{\partial t} + u\frac{\partial u}{\partial x} + v\frac{\partial u}{\partial y} = -\frac{\partial p}{\partial x} + \frac{\partial^2 u}{\partial y^2} + \frac{Gr}{Re^2}\sin(\theta)T, \tag{2.5a}$$

$$0 = -\frac{\partial p}{\partial y} + \frac{Gr}{Re^{5/2}}\cos(\theta)T, \tag{2.5b}$$

$$\frac{\partial T}{\partial t} + u\frac{\partial T}{\partial x} + v\frac{\partial T}{\partial y} = \frac{1}{Pr}\frac{\partial^2 T}{\partial y^2}, \tag{2.5c}$$

$$\frac{\partial u}{\partial x} + \frac{\partial v}{\partial y} = 0, \tag{2.5d}$$

where $Pr = \nu/\alpha$ is the Prandtl number, and $Gr = g\beta(T_s - T_\infty)L^3/\nu^2$ is the Grashof number. The boundary conditions (2.3) become

$$u = -1, \quad v = 0, \quad T = 1 \quad \text{at } y = 0, \tag{2.6a}$$

$$u \to U_\infty(x), \quad T \to 0 \quad \text{as } y \to \infty. \tag{2.6b}$$

The pressure gradient term in (2.5*a*) may be expressed in terms of the mainstream velocity distribution which is prescribed by (2.1). The momentum equation in the direction normal to the wall (2.5*b*) produces a balance between the normal pressure gradient and the buoyancy force in the normal direction, which is $O(Gr/Re^{5/2})$. Alternatively, the normal buoyancy force can be shown to induce a streamwise pressure gradient (see, for example, Schneider & Wasel 1985). Integrating (2.5*b*) across the boundary layer and then differentiating with respect to x gives

$$\frac{\partial p}{\partial x} = \frac{Gr}{Re^{5/2}}\cos\theta\frac{\partial}{\partial x}\int_y^\infty T\,\mathrm{d}y. \tag{2.7}$$

This contribution to the streamwise pressure gradient can be combined with that from the inviscid flow, written in terms of the mainstream velocity, to give the following form of the streamwise momentum equation:

$$\frac{\partial u}{\partial t} + u\frac{\partial u}{\partial x} + v\frac{\partial u}{\partial y} = U_\infty\frac{\mathrm{d}U_\infty}{\mathrm{d}x} - \frac{Gr}{Re^{5/2}}\cos\theta\frac{\partial}{\partial x}\int_y^\infty T\,\mathrm{d}y + \frac{\partial^2 u}{\partial y^2} + \frac{Gr}{Re^2}\sin(\theta)T, \tag{2.8}$$

which, along with the energy equation (2.5*c*) and continuity equation (2.5*d*), is an alternative formulation of the mixed-convection boundary-layer equations.

If the surface is horizontal, i.e. $\theta = 0^\circ$ or $\theta = 180^\circ$, the last term in (2.8) vanishes, and there is no buoyancy force in the streamwise direction. For this orientation of the surface, one can consider a case with $Gr/Re^{5/2} \to 0$, resulting in forced convection, or $Gr/Re^{5/2} = O(1)$, for which the buoyancy force in the normal direction induces a streamwise pressure gradient as shown in (2.7). If the full range of inclination angles is to be considered, the streamwise pressure gradient due to the buoyancy force normal to the surface, which is $O(Gr/Re^{5/2})$, is small compared to the buoyancy force in the streamwise direction, which is $O(Gr/Re^2)$, as $Re \to \infty$. Therefore, we have forced convection for all inclination angles θ if $Gr/Re^2 \to 0$. In this investigation, however, it is of interest to consider the influence of mixed convection for the full range of inclination angles; therefore, it is assumed that the buoyancy force in the streamwise direction is of the same order as the inertial terms in the momentum equation, i.e. $Gr/Re^2 = O(1)$, which results in there being no contribution to the pressure gradient resulting from the normal buoyancy force. In addition, the case with $Pr = O(1)$ is considered; therefore, the momentum and thermal boundary layers have the same order of thickness.

The flow is initiated in an impulsive start at $t = 0$, after which a boundary layer forms along the surface which thickens proportional to $t^{1/2}$. Therefore, Rayleigh variables are introduced as follows:

$$\zeta = \frac{y}{2t^{1/2}}, \quad \Psi = \frac{\psi}{2t^{1/2}}, \tag{2.9a,b}$$

where ψ is the streamfunction defined by $u = \partial\psi/\partial y, v = -\partial\psi/\partial x$. Substitution of these variables into the governing equations (2.8), with $Gr/Re^{5/2} \to 0$, and (2.5c) gives the following set of equations:

$$4t\frac{\partial u}{\partial t} = \frac{\partial^2 u}{\partial \zeta^2} + 2\zeta\frac{\partial u}{\partial \zeta} + 4t\left[\frac{\partial \Psi}{\partial x}\frac{\partial u}{\partial \zeta} - u\frac{\partial u}{\partial x} + U_\infty\frac{dU_\infty}{dx} + \frac{Gr}{Re^2}\sin(\theta)T\right], \tag{2.10a}$$

$$4t\frac{\partial T}{\partial t} = \frac{1}{Pr}\frac{\partial^2 T}{\partial \zeta^2} + 2\zeta\frac{\partial T}{\partial \zeta} + 4t\left[\frac{\partial \Psi}{\partial x}\frac{\partial T}{\partial \zeta} - u\frac{\partial T}{\partial x}\right], \tag{2.10b}$$

$$u = \frac{\partial \Psi}{\partial \zeta}, \tag{2.10c}$$

and the boundary conditions (2.6) become

$$u = -1, \quad \Psi = 0, \quad T = 1 \quad \text{at } \zeta = 0, \tag{2.11a}$$

$$u \to U_\infty(x), \quad T \to 0 \quad \text{as } \zeta \to \infty. \tag{2.11b}$$

The initial conditions are obtained by evaluating equations (2.10) as $t \to 0$ and solving the resulting equations subject to the boundary conditions (2.11). This results in

$$u = (U_\infty + 1)\text{erf}(\zeta) - 1, \quad T = 1 - \text{erf}(Pr^{1/2}\zeta), \tag{2.12a, b}$$

$$\Psi = (U_\infty + 1)[\zeta\text{erf}(\zeta) - \pi^{-1/2}(1 - e^{-\zeta^2})] - \zeta, \tag{2.12c}$$

at $t = 0$. Similarly, the boundary conditions at upstream and downstream infinity are obtained by considering equations (2.10) as $x \to \pm\infty$, where the streamwise gradients go to zero. The resulting energy equation is the same as that for the initial condition; therefore, equation (2.12b) is the boundary condition as $x \to \pm\infty$. Due to natural convection, however, the streamwise velocity at upstream and downstream infinity must be computed from

$$4t\frac{\partial u}{\partial t} = \frac{\partial^2 u}{\partial \zeta^2} + 2\zeta\frac{\partial u}{\partial \zeta} + 4t\frac{Gr}{Re^2}\sin(\theta)T, \tag{2.13}$$

subject to the boundary conditions (2.11). Here T is given by (2.12b).

For computational purposes it is convenient to transform the semi-infinite physical domain ($-\infty \leqslant x \leqslant \infty, 0 \leqslant \zeta \leqslant \infty$) to a finite domain ($0 \leqslant \hat{x} \leqslant 2, 0 \leqslant \hat{\zeta} \leqslant 1$) using the transformations

$$\hat{x} = 1 - \frac{2}{\pi}\arctan\left(\frac{x}{a}\right), \quad \hat{\zeta} = \frac{2}{\pi}\arctan\left(\frac{\zeta}{b}\right). \tag{2.14a, b}$$

Reducing the parameters a and b concentrates more grid points in the physical grid near $x = 0$ and $\zeta = 0$, respectively, providing greater resolution along the wall and immediately beneath the centre of the vortex. Application of these transformations to (2.10) gives the Eulerian formulation in its final form as

$$4t\frac{\partial u}{\partial t} = P\frac{\partial^2 u}{\partial \hat{\zeta}^2} + (Q_1 + Q_2)\frac{\partial u}{\partial \hat{\zeta}} + R\frac{\partial u}{\partial \hat{x}} + S, \tag{2.15a}$$

$$4t\frac{\partial T}{\partial t} = \frac{P}{Pr}\frac{\partial^2 T}{\partial \hat{\zeta}^2} + \left(\frac{Q_1}{Pr} + Q_2\right)\frac{\partial T}{\partial \hat{\zeta}} + R\frac{\partial T}{\partial \hat{x}}, \tag{2.15b}$$

$$u = \Gamma_\zeta(\hat{\zeta})\frac{\partial \Psi}{\partial \hat{\zeta}}, \tag{2.15c}$$

where the coefficients are

$$P(\hat{\zeta}) = \Gamma_{\zeta}^{2}(\hat{\zeta}), \tag{2.16a}$$

$$Q_1(\hat{\zeta}) = \Gamma_{\zeta}(\hat{\zeta})\Gamma_{\zeta}'(\hat{\zeta}), \tag{2.16b}$$

$$Q_2(\hat{x}, \hat{\zeta}, t) = 2b \tan\left(\frac{\pi\hat{\zeta}}{2}\right)\Gamma_{\zeta}(\hat{\zeta}) + 4t\Gamma_{\zeta}(\hat{\zeta})\Gamma_{x}(\hat{x})\frac{\partial \Psi}{\partial \hat{x}}, \tag{2.16c}$$

$$R(\hat{x}, \hat{\zeta}, t) = -4t\Gamma_{x}(\hat{x})u, \tag{2.16d}$$

$$S(\hat{x}, \hat{\zeta}, t) = 4t\left[U_{\infty}\frac{\mathrm{d}U_{\infty}}{\mathrm{d}x} + \frac{Gr}{Re^{2}}\sin(\theta)T\right]. \tag{2.16e}$$

In the above expressions Γ_x and Γ_ζ are defined by

$$\Gamma_{x}(\hat{x}) = -\frac{1}{\pi a}[1 - \cos(\pi\hat{x})], \quad \Gamma_{\zeta}(\hat{\zeta}) = \frac{1}{\pi b}[1 + \cos(\pi\hat{\zeta})]. \tag{2.17a, b}$$

The initial conditions (2.12) and the boundary conditions (2.11) and (2.13) are likewise written in terms of $\hat{x}$ and $\hat{\zeta}$.

Starting at $t = 0$, an iteration is carried out on the coupled equations (2.15) at each time step until the relative difference between the dependent variables, i.e. $u(\hat{x}, \hat{\zeta}, t)$, $T(\hat{x}, \hat{\zeta}, t)$ and $\Psi(\hat{x}, \hat{\zeta}, t)$, at successive iterates is less than some tolerance value. The momentum and energy equations are solved on a uniform grid in computational space $(\hat{x}, \hat{\zeta})$ using a factored ADI method similar to that described by Peridier *et al.* (1991*a*), and the streamfunction is determined by integration of (2.15*c*) using Simpson's rule. The factored ADI method is second-order accurate in both space and time and utilizes a Crank–Nicolson approach for the time stepping in which quantities are evaluated midway between the current and previous time steps. The algorithm also employs second-order-accurate upwind-downwind differencing of the first-order derivatives in order to ensure diagonal dominance of the tridiagonal matrix problems which arise from the discretization of the governing equations. The method has been found to work well in obtaining solutions of unsteady two-dimensional problems in which severe gradients develop locally, in particular flows involving unsteady separation.

Previous attempts to compute the classical boundary-layer equations subject to an adverse pressure gradient in the Eulerian formulation have proven to be very difficult (see, for example, Walker 1978). For the case of the vortex-induced boundary layer being considered here, it has been shown that a region of recirculating flow develops within the boundary layer as a result of the adverse pressure gradient. As the boundary layer evolves, the recirculation region grows in size and induces strong outflows normal to the surface on the upstream side of the recirculating eddy. As these outflows become progressively more intense, and consequently more difficult to resolve, the numerical calculation breaks down; Walker (1978) found that this occurs at approximately $t = 0.75$. It has become apparent from several attempts to compute similar flows that numerical schemes using the conventional Eulerian formulation and fixed grids are unable to accurately resolve the latter stages of such eruptive events. Instead it is necessary to use adaptive grids, as demonstrated by Adams, Conlisk & Smith (1995) and Xiao, Adams & Conlisk (1996), or to calculate the Lagrangian formulation of the unsteady boundary-layer equations.

Due to the difficulties associated with obtaining numerical solutions of boundary-layer flows involving unsteady separation in conventional Eulerian coordinates, the

mixed-convection boundary-layer equations are reformulated in Lagrangian coordinates as shown in the next section. This approach has been found to be effective for the vortex-induced boundary-layer flow without heat transfer (Peridier *et al.* 1991*a*) and the flow over an impulsively-started circular cylinder (Van Dommelen & Shen 1982), which exhibits similar eruptive behaviour. In this investigation, as in Peridier *et al.* (1991*a*), numerical solutions of the Eulerian formulation are performed immediately following the impulsive start to capture the thickening Rayleigh layer. The calculations then switch over to the Lagrangian formulation in order to accurately resolve the latter stages of the separation process, including the singularity.

2.2. *Lagrangian formulation*

In the Lagrangian description of fluid motion, the trajectories of the fluid particles are determined as functions of their initial locations and time. Taking ξ to be the initial streamwise location and η to be the initial normal location of the fluid particles at some time $t = t_0$, the dependent variables are the streamwise and normal particle positions $x = x(\xi, \eta, t)$ and $y = y(\xi, \eta, t)$, respectively, and the corresponding velocity components $u = u(\xi, \eta, t)$ and $v = v(\xi, \eta, t)$. In Lagrangian coordinates the boundary-layer equation (2.8) becomes

$$\frac{\partial u}{\partial t} = U_\infty \frac{\mathrm{d}U_\infty}{\mathrm{d}x} + \left[\frac{\partial x}{\partial \xi}\frac{\partial}{\partial \eta} - \frac{\partial x}{\partial \eta}\frac{\partial}{\partial \xi}\right]^2 u + \frac{Gr}{Re^2}\sin(\theta)T, \tag{2.18a}$$

where

$$\frac{\partial x}{\partial t} = u. \tag{2.18b}$$

Similarly, the energy equation (2.5*c*) becomes

$$\frac{\partial T}{\partial t} = \frac{1}{Pr}\left[\frac{\partial x}{\partial \xi}\frac{\partial}{\partial \eta} - \frac{\partial x}{\partial \eta}\frac{\partial}{\partial \xi}\right]^2 T. \tag{2.18c}$$

Note that the pressure gradient term, i.e. the first term on the right-hand side of (2.18*a*), is expressed in terms of the current streamwise particle position $x(\xi, \eta, t)$. One of the primary advantages of the Lagrangian formulation of the boundary-layer equations is evident from (2.18). Observe that the momentum and energy equations do not involve the particle positions $y(\xi, \eta, t)$ and velocities $v(\xi, \eta, t)$ normal to the surface; it is these quantities that become large, and in fact singular, as a boundary-layer eruption occurs. Equations (2.18), therefore, may be used to calculate the streamwise particle position $x(\xi, \eta, t)$, the streamwise velocity $u(\xi, \eta, t)$ and the temperature $T(\xi, \eta, t)$, quantities which remain finite even as $y(\xi, \eta, t)$ and $v(\xi, \eta, t)$ become singular.

In order to resolve the Rayleigh layer, it is convenient to compute the initial stages of the flow after the impulsive start at $t = 0$ using the Eulerian formulation given in the previous section and then switch over to the Lagrangian formulation at some time t_0. Therefore, the initial conditions for the Lagrangian calculation are

$$x(\xi, \eta, t) = \xi, \quad u(\xi, \eta, t) = u_0(\xi, \eta), \quad T(\xi, \eta, t) = T_0(\xi, \eta) \quad \text{at } t = t_0, \tag{2.19}$$

where $u_0(\xi, \eta)$ and $T_0(\xi, \eta)$ are the streamwise velocity and temperature distributions at $t = t_0$ from the Eulerian calculation. The boundary conditions at the wall and as the mainstream is approached are

$$u = -1, \quad T = 1 \qquad \text{at } \eta = 0, \tag{2.20a}$$

$$u \to U_\infty(x), \quad T \to 0 \qquad \text{as } \eta \to \infty. \tag{2.20b}$$

The flow at upstream and downstream infinity is plane parallel; therefore, $y = \eta$ for all t, and from (2.12b) with (2.9)

$$T = 1 - \mathrm{erf}\left(Pr^{1/2} \frac{\eta}{2t^{1/2}} \right) \quad \text{as } \xi \to \pm\infty. \tag{2.21}$$

The corresponding streamwise velocity boundary conditions are determined by solving

$$\frac{\partial u}{\partial t} = \frac{\partial^2 u}{\partial \eta^2} + \frac{Gr}{Re^2} \sin(\theta) T, \tag{2.22}$$

where T is given by (2.21). This equation takes into account the natural convection occurring at upstream and downstream infinity.

At any stage during the integration of the momentum and energy equations (2.18), the normal particle positions $y(\xi, \eta, t)$ may be determined from a solution of the continuity equation, which in Lagrangian coordinates takes the form

$$\frac{\partial x}{\partial \xi}\frac{\partial y}{\partial \eta} - \frac{\partial x}{\partial \eta}\frac{\partial y}{\partial \xi} = 1, \tag{2.23}$$

for incompressible flows. Equation (2.23) indicates that the Jacobian of the particle positions remains equal to one. The streamwise particle positions $x(\xi, \eta, t)$ at a given time are known from a solution of (2.18); therefore, the continuity equation (2.23) is a first-order linear partial differential equation for the normal particle positions $y(\xi, \eta, t)$. Solutions of the continuity equation at a given time are obtained by integrating along curves of constant x having the characteristic equations

$$\frac{\mathrm{d}\xi}{-\partial x/\partial \eta} = \frac{\mathrm{d}\eta}{\partial x/\partial \xi} = \mathrm{d}y. \tag{2.24}$$

This integration is performed using a predictor–corrector algorithm similar to that described by Peridier *et al.* (1991*a*). The integration is initiated at the wall, where the particle positions are known due to the no-slip condition, and proceeds along the characteristics to the outer edge of the boundary layer. When plotted on the (ξ, η)-plane, a curve of constant x represents the initial positions of a set of fluid particles which at the current time are located along the vertical line $\xi = x =$ constant.

A singularity occurs in the boundary-layer equations when a fluid particle initially located within the boundary layer is at some time t_s located an infinite distance from the surface (on the boundary-layer scale). This occurs when a stationary point develops in the x-field indicated by

$$\frac{\partial x}{\partial \xi} = \frac{\partial x}{\partial \eta} = 0 \quad \text{at } \xi = \xi_s, \ \ \eta = \eta_s, \ \ t = t_s. \tag{2.25}$$

This criterion for the formation of a singularity is clear and unambiguous and marks a second advantage of Lagrangian calculations over those carried out in Eulerian coordinates, for which the criterion for a singularity is very difficult to evaluate numerically. In order to detect the onset of a singularity, the $\partial x/\partial \xi = 0$ and $\partial x/\partial \eta = 0$ curves are tracked during the calculation in a manner similar to that used by Degani *et al.* (1998) to determine the time and location where they first intersect. The onset of a singularity indicates that a fluid particle initially located at (ξ_s, η_s) has at time t_s been compressed to zero thickness in the streamwise direction and expanded to infinite thickness in the normal direction due to conservation of mass for an incompressible fluid. Such an occurrence violates the assumption that the boundary layer remains thin and does not interact with the outer inviscid flow, thus resulting in a singularity.

Just as in the Eulerian formulation, the domain is transformed to a finite region ($0 \leqslant \hat{\xi} \leqslant 2, 0 \leqslant \hat{\eta} \leqslant 1$) using transformations similar to (2.14), namely

$$\hat{\xi} = 1 - \frac{2}{\pi} \arctan\left(\frac{\xi}{a}\right), \quad \hat{\eta} = \frac{2}{\pi} \arctan\left(\frac{\eta}{b}\right), \tag{2.26a,b}$$

with analogous transformations for the dependent variables $x(\xi, \eta, t)$ and $y(\xi, \eta, t)$. Applying these transformations to the governing equations (2.18) and (2.23) gives

$$\frac{\partial u}{\partial t} = P\frac{\partial^2 u}{\partial \hat{\eta}^2} + W\frac{\partial^2 u}{\partial \hat{\xi}^2} + Z\frac{\partial^2 u}{\partial \hat{\xi}\partial \hat{\eta}} + Q\frac{\partial u}{\partial \hat{\eta}} + R\frac{\partial u}{\partial \hat{\xi}} + S, \tag{2.27a}$$

$$\frac{\partial \hat{x}}{\partial t} = \Gamma_{\xi}(\hat{x})u, \tag{2.27b}$$

$$\frac{\partial T}{\partial t} = \frac{1}{Pr}\left[P\frac{\partial^2 T}{\partial \hat{\eta}^2} + W\frac{\partial^2 T}{\partial \hat{\xi}^2} + Z\frac{\partial^2 T}{\partial \hat{\xi}\partial \hat{\eta}} + Q\frac{\partial T}{\partial \hat{\eta}} + R\frac{\partial T}{\partial \hat{\xi}}\right], \tag{2.27c}$$

$$\frac{\partial \hat{x}}{\partial \hat{\xi}}\frac{\partial \hat{y}}{\partial \hat{\eta}} - \frac{\partial \hat{x}}{\partial \hat{\eta}}\frac{\partial \hat{y}}{\partial \hat{\xi}} = \frac{\Gamma_{\xi}(\hat{x})\Gamma_{\eta}(\hat{y})}{\Gamma_{\xi}(\hat{\xi})\Gamma_{\eta}(\hat{\eta})}, \tag{2.27d}$$

where the coefficients in (2.27a, c) are given by

$$P = \gamma\left(\frac{\partial \hat{x}}{\partial \hat{\xi}}\right)^2, \quad W = \gamma\left(\frac{\partial \hat{x}}{\partial \hat{\eta}}\right)^2, \quad Z = -2\gamma\frac{\partial \hat{x}}{\partial \hat{\xi}}\frac{\partial \hat{x}}{\partial \hat{\eta}}, \tag{2.28a–c}$$

$$Q = \gamma\left[\frac{\Gamma_{\eta}'(\hat{\eta})}{\Gamma_{\eta}(\hat{\eta})}\left(\frac{\partial \hat{x}}{\partial \hat{\xi}}\right)^2 + \frac{\partial \hat{x}}{\partial \hat{\xi}}\frac{\partial^2 \hat{x}}{\partial \hat{\xi}\partial \hat{\eta}} - \frac{\Gamma_{\xi}'(\hat{\xi})}{\Gamma_{\xi}(\hat{\xi})}\frac{\partial \hat{x}}{\partial \hat{\xi}}\frac{\partial \hat{x}}{\partial \hat{\eta}} - \frac{\partial \hat{x}}{\partial \hat{\eta}}\frac{\partial^2 \hat{x}}{\partial \hat{\xi}^2}\right], \tag{2.28d}$$

$$R = \gamma\left[\frac{\Gamma_{\xi}'(\hat{\xi})}{\Gamma_{\xi}(\hat{\xi})}\left(\frac{\partial \hat{x}}{\partial \hat{\eta}}\right)^2 + \frac{\partial \hat{x}}{\partial \hat{\eta}}\frac{\partial^2 \hat{x}}{\partial \hat{\xi}\partial \hat{\eta}} - \frac{\Gamma_{\eta}'(\hat{\eta})}{\Gamma_{\eta}(\hat{\eta})}\frac{\partial \hat{x}}{\partial \hat{\xi}}\frac{\partial \hat{x}}{\partial \hat{\eta}} - \frac{\partial \hat{x}}{\partial \hat{\xi}}\frac{\partial^2 \hat{x}}{\partial \hat{\eta}^2}\right], \tag{2.28e}$$

$$S = U_{\infty}\frac{\mathrm{d}U_{\infty}}{\mathrm{d}x} + \frac{Gr}{Re^2}\sin(\theta)T. \tag{2.28f}$$

Here a prime denotes an ordinary derivative with respect to the indicated variable. The coefficient γ is defined by

$$\gamma(\hat{x}, \hat{\xi}, \hat{\eta}) = \left[\frac{\Gamma_{\xi}(\hat{\xi})}{\Gamma_{\xi}(\hat{x})}\Gamma_{\eta}(\hat{\eta})\right]^2, \tag{2.29}$$

and Γ_{ξ} and Γ_{η} are given by

$$\Gamma_{\xi}(\hat{\xi}) = -\frac{1}{\pi a}[1 - \cos(\pi\hat{\xi})], \quad \Gamma_{\eta}(\hat{\eta}) = \frac{1}{\pi b}[1 + \cos(\pi\hat{\eta})]. \tag{2.30a,b}$$

The boundary conditions (2.20)–(2.22) are likewise transformed using (2.26).

As discussed previously, the initial stages of the flow after the impulsive start are calculated using the Eulerian formulation described in the previous section until some time $t = t_0$ at which time the Lagrangian calculation is initiated. It is convenient to define the initial conditions for the particle positions to be coincident with the Eulerian mesh at the switch-over time t_0; therefore,

$$\hat{\xi} = \hat{x}, \quad \hat{\eta} = \hat{\zeta} \qquad \text{at } t = t_0. \tag{2.31}$$

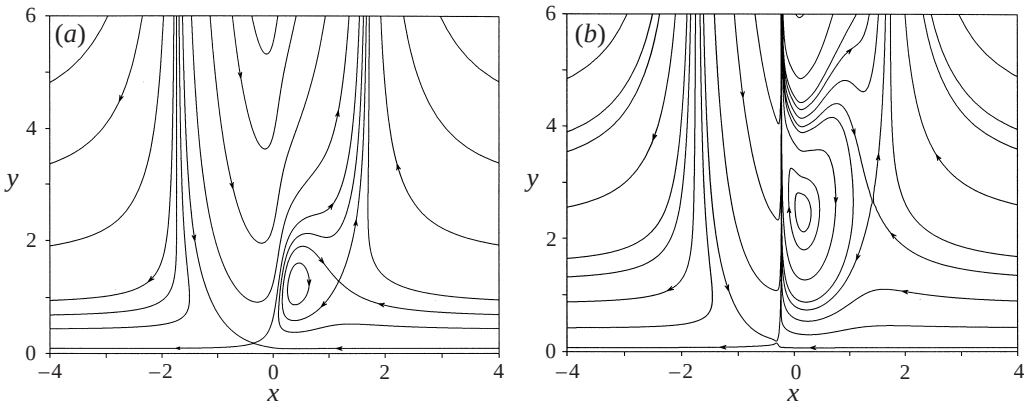

FIGURE 2. Instantaneous streamlines for the forced-convective case. (*a*) $t = 0.5$, (*b*) $t = t_s = 1.0127$.

The first of these conditions is accomplished by using the same transformations on the streamwise coordinate in both the Eulerian and Lagrangian formulations. In order for the second condition to be satisfied, recall that ζ is a Rayleigh variable in the Eulerian formulation defined by $\zeta = y/2t^{1/2}$. Therefore, taking b_ζ to be the stretching parameter in the transformation used in the Eulerian formulation and b_η to be that used in the Lagrangian formulation, (2.31) is satisfied if b_η is chosen such that

$$b_\eta = 2t_0^{1/2} b_\zeta. \tag{2.32}$$

Accomplishing the switch over to the Lagrangian calculation in this way does not require any interpolation of the Eulerian solution. Here the switch-over time is chosen to be $t_0 = 0.25$, in which case $b_\eta = b_\zeta$; however, other values also have been tested to ensure that the solutions are independent of the choice of t_0. In order to advance the solution in Lagrangian coordinates, equations (2.27*a–c*) are solved using an algorithm similar to that used to solve (2.15) in the Eulerian formulation (Peridier *et al.* 1991*a*).

3. Numerical results

In general, equations (2.15) (or equations (2.27) in Lagrangian coordinates) are coupled, and the momentum and energy equations must be solved simultaneously. When the surface is horizontal ($\theta = 0°, 180°$), however, there is no buoyancy force in the streamwise direction, and the fluid flow becomes uncoupled from the heat transfer leading to a forced-convective flow. This is a consequence of considering the parameter range where $Gr/Re^2 = O(1)$ due to our interest in computing the flow for all angles of inclination. If one were only considering the horizontal case, it would be possible to consider another parameter range where $Gr/Re^{5/2} = O(1)$ in which case the buoyancy force in the normal direction induces a streamwise pressure gradient as shown in equation (2.8).

For the forced-convective case, with $\theta = 0°, 180°$, the numerical results obtained here for the flow field are the same as those given by Peridier *et al.* (1991*a*) in which the boundary layer develops a secondary recirculation region due to the adverse pressure gradient induced by the vortex. The secondary eddy is shown in figure 2(*a*), which shows the instantaneous streamlines on the boundary-layer scale at time $t = 0.5$. All results shown are for $Pr = 1$ and, unless stated otherwise, have been obtained on a uniform mesh in $(\hat{\xi}, \hat{\eta})$ composed of 201 and 101 grid points in the streamwise and

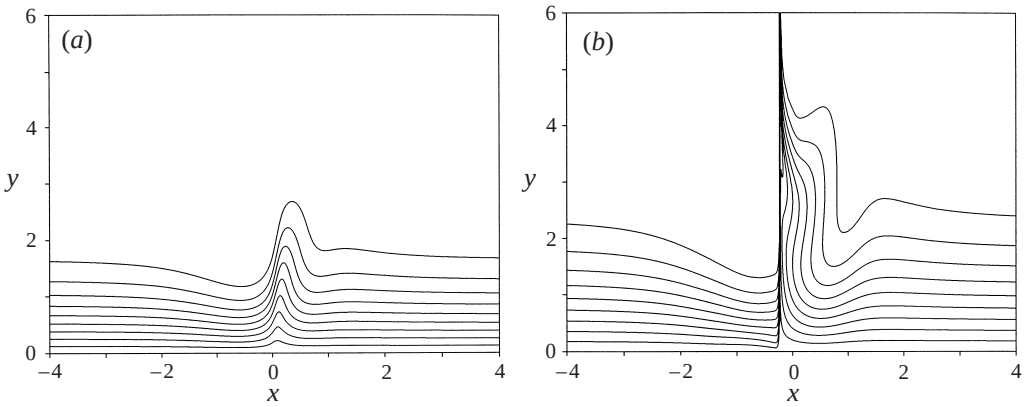

FIGURE 3. Isotherms in increments of $T = 0.1$ for the forced-convective case. (*a*) $t = 0.5$, (*b*) $t = t_s = 1.0127$.

normal directions, respectively, with the stretching parameters in the transformations being set to $a = b = 1$. Calculations also have been performed on finer grids, up to 401×201, and using different values of the stretching parameters in order to ensure grid independence. As the boundary layer evolves, the spatial extent of the recirculation region grows, in particular in the direction normal to the surface. The presence of this growing recirculating eddy acts as a barrier to the oncoming flow, an effect which is accentuated by its 'ploughing' motion upstream, and results in a strong focusing of the flow in a narrow streamwise region on the upstream side of the eddy. In the region between the inviscid stagnation points at $x = \pm\sqrt{3}$, the boundary-layer flow is from left to right; therefore, motion to the left within this region is said to be upstream. Figure 2(*b*) shows the instantaneous streamlines at time $t_s = 1.0127$ at which a singularity occurs in the boundary-layer equations at $x_s = -0.22$. Note that the slight difference in singularity time compared to that determined by Peridier *et al.* (1991*a*) is attributed to the different methods used to determine the singularity time as described in § 2.2. The onset of the singularity signals that the boundary-layer assumptions, namely that the boundary layer remains thin and has negligible influence on the outer inviscid flow, break down locally near the eruption.

As one would expect, this locally erupting flow has a dramatic effect upon the convective heat transfer within the boundary layer. The constant-temperature contours in figure 3(*a*) at $t = 0.5$ (corresponding to figure 2*a*) show that the outflows induced within the boundary layer by the secondary eddy cause the heated near-wall fluid to be convected away from the surface leading to the development of a high-temperature plume. In the latter stages of the calculation, the formation of the singularity results in an abrupt eruption of high-vorticity, high-temperature fluid from adjacent to the surface in a very narrow region near $x_s = -0.22$ as shown in figure 3(*b*). The singularity occurs on the upstream side of the secondary eddy and the corresponding high-temperature plume and results in very large temperature gradients in this region.

In addition to having a pronounced effect upon the convective heat transfer within the boundary layer, this eruptive behaviour also induces large variations in the heat transfer from the heated surface. The temporal evolution of the convective heat transfer coefficient $h = -(\partial T/\partial y)_{y=0}$ is shown in figure 4. The convective heat transfer coefficient upstream and downstream of the eruptive region decreases with time due to the thickening of the overall boundary layer following the impulsive start, and the

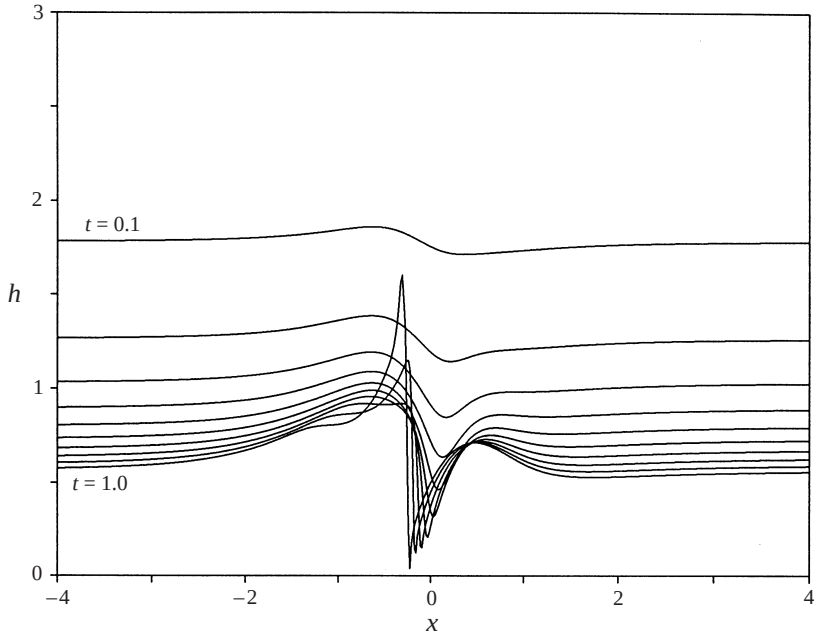

FIGURE 4. Temporal development in increments of $t = 0.1$ of the convective heat transfer coefficient for the forced-convective case.

thermal gradients become less pronounced as the heat diffuses away from the surface. In the region beneath the centre of the vortex near $x = 0$, a local minimum in the heat transfer coefficient begins to develop as a result of the convection of the heated fluid away from the surface forming the high-temperature plume. As the singularity time is approached, this local minimum intensifies, and a local maximum also appears just upstream of the separation point as a result of the inflow from the outer portion of the boundary layer just upstream of the secondary recirculation region (see figure 2*b*). Although not as pronounced, this type of behaviour in the surface heat flux was also observed by Puhak *et al.* (1995) who considered the boundary-layer flow upstream of obstacles which exhibit similar eruptive behaviour. It has also been observed in gravity current flows where the vortices spawned from the advancing head interact with the surface and cause locally eruptive behaviour producing sharp spikes in the heat transfer from the wall (Rehm *et al.* 1995).

Thus far the forced-convective case has been considered in which the heat transfer has no influence upon the fluid flow. Next it is of interest to consider the case when the surface is inclined from the horizontal so that the buoyancy force in the streamwise direction is non-zero, and the flow field and heat transfer are coupled, i.e. the mixed-convection case. A series of calculations has been carried out for the full range of inclination angles ($0^\circ < \theta < 360^\circ$) in increments of 15° with a fixed value of $Gr/Re^2 = 4$. Results for the time t_s at which the singularity occurs and the streamwise position x_s and speed u_s of the singular point are given in figure 5. The values given for $\theta = 0^\circ, 180^\circ$ and 360° represent the forced-convective case. Although this is a strongly forced environment, it is clear that the effect of even moderate buoyancy on the flow field can be very significant. Notice in particular that for $0^\circ < \theta < 180^\circ$, the time at which the singularity occurs is delayed, separation occurs farther downstream, and the magnitude of the local streamwise velocity at

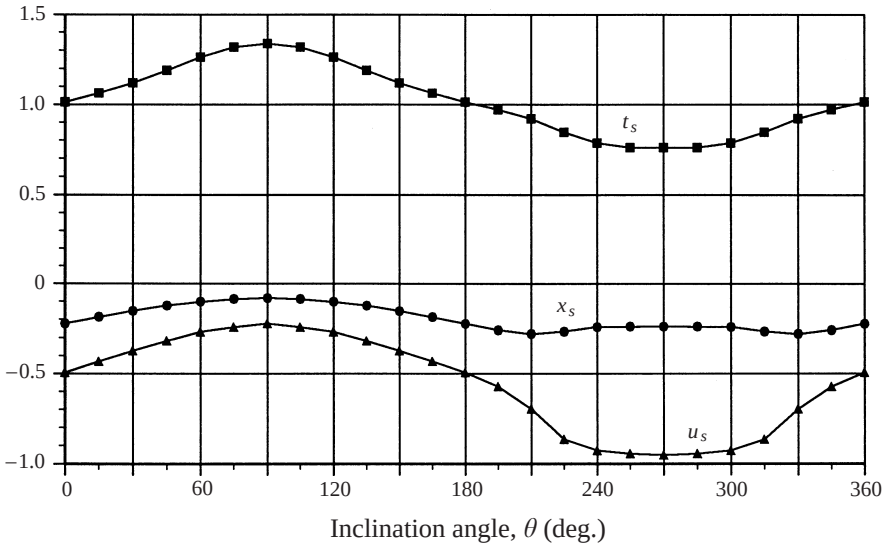

FIGURE 5. Singularity time t_s, position x_s and speed u_s for $Gr/Re^2 = 4$ and various inclination angles in increments of 15°.

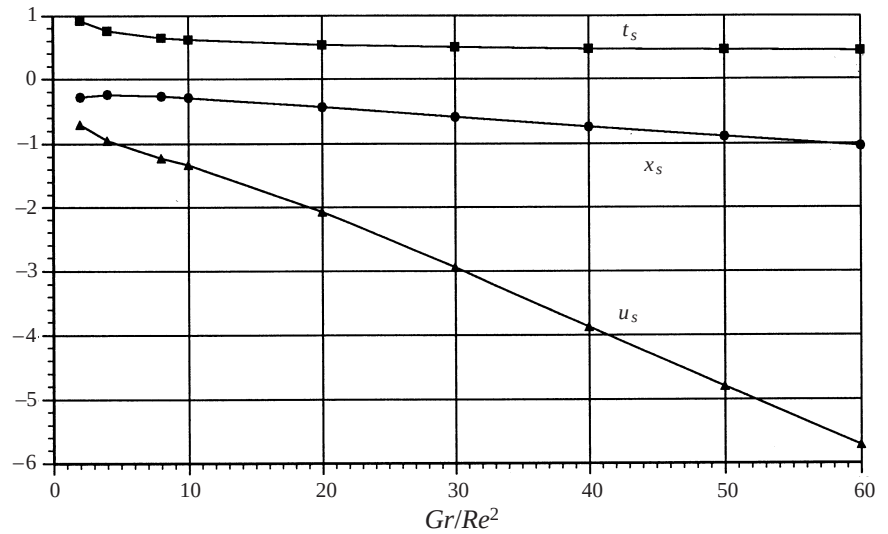

FIGURE 6. Singularity time t_s, position x_s and speed u_s for $\theta = 270°$ and various Gr/Re^2.

separation is smaller. For $180° < \theta < 360°$, on the other hand, the onset of the singularity is accelerated by the action of buoyancy forces, and while the streamwise position of separation changes very little, the magnitude of the local velocity increases significantly. For the cases with $0° < \theta < 180°$, the buoyancy force acts in the positive x-direction and counteracts the effects of the adverse pressure gradient, dampening its influence on the boundary-layer flow. For $180° < \theta < 360°$, the buoyancy force acts in the same direction as the adverse pressure gradient, i.e. the negative x-direction, accelerating the separation process.

The buoyancy force has its greatest influence when the surface is vertical, i.e. $\theta = 90°$ or $\theta = 270°$, and it is of interest to consider these cases in more detail. It might be

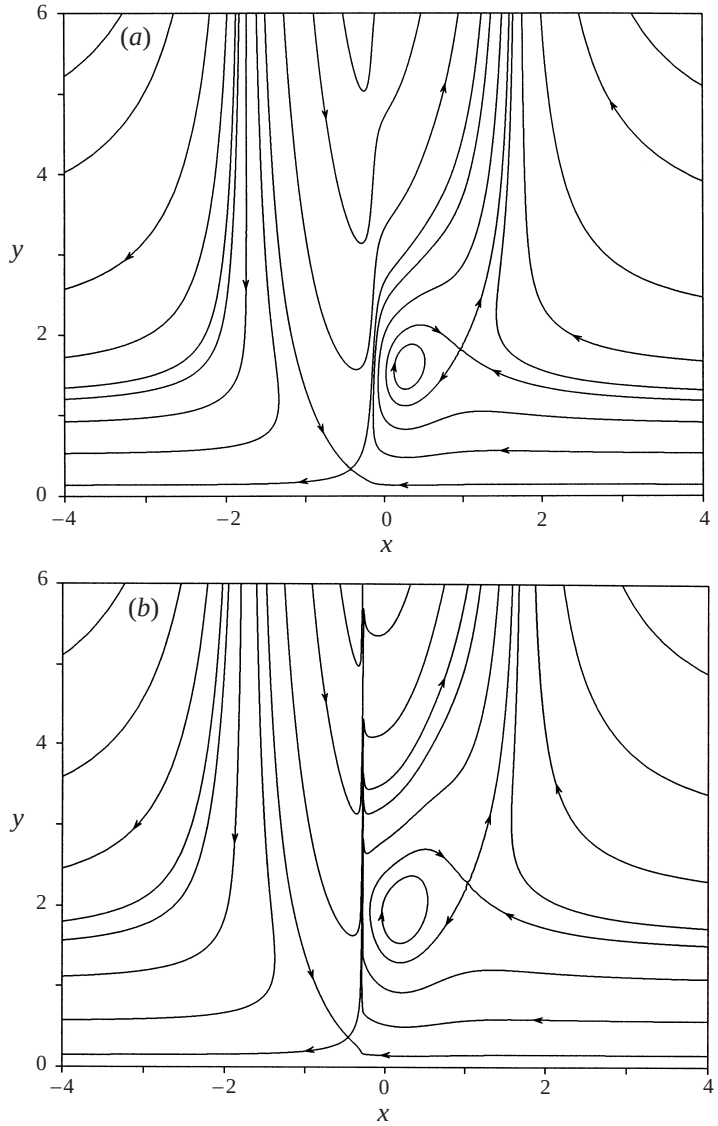

FIGURE 7. Instantaneous streamlines for $\theta = 270°$, $Gr/Re^2 = 10$. (*a*) $t = 0.5$, (*b*) $t = t_s = 0.6192$.

expected that the trends observed in figure 5 would continue for fixed inclination angles and increasing values of the buoyancy force. Indeed for $\theta = 270°$, for which the buoyancy force accelerates the separation process, the trends stated above continue for increasing Gr/Re^2 as shown in figure 6. For example, the streamlines for the case with $Gr/Re^2 = 10$ are shown in figure 7 at $t = 0.5$ and $t = t_s = 0.6192$. For this case the secondary recirculation region appears slightly later in time and farther from the surface compared to the forced-convective case (cf. figure 2*a*). However, the point that becomes singular travels upstream more rapidly, i.e. $|u_s(\theta = 270°)| > |u_s(\theta = 0°)|$, hastening the onset of the singularity. The reason for this can be observed from the isotherms shown in figure 8. The isotherms at $t = 0.5$, shown in figure 8(*a*), appear very similar to those at the corresponding time in the forced-convective case (cf.

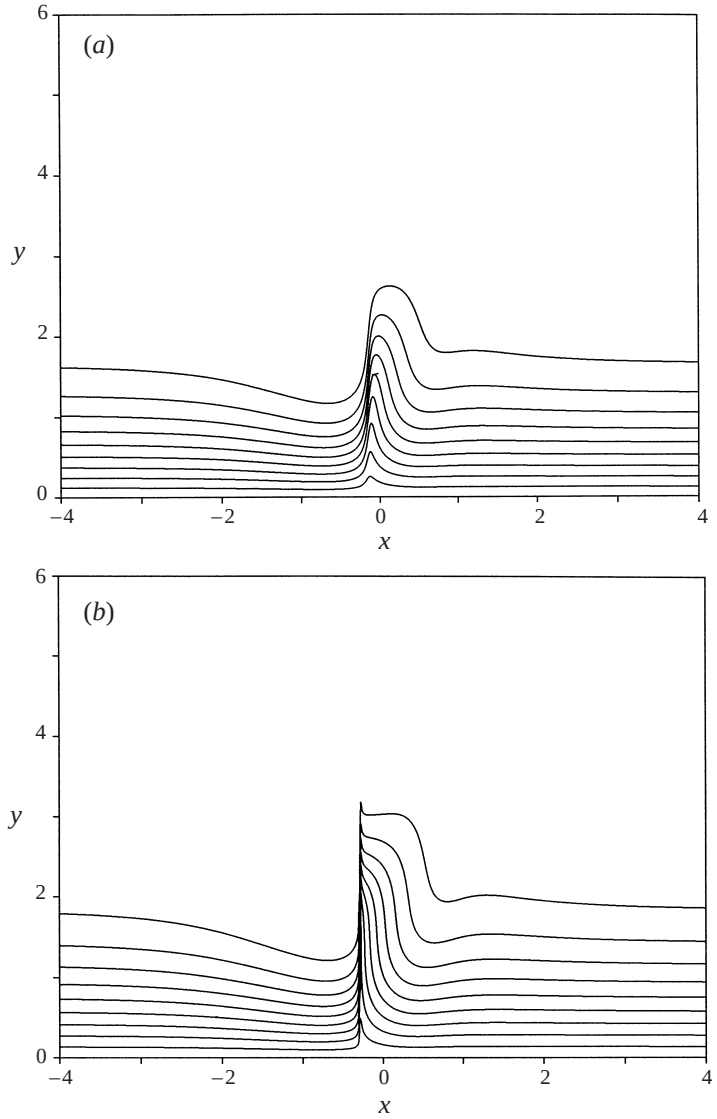

FIGURE 8. Isotherms in increments of $T = 0.1$ for $\theta = 270°$, $Gr/Re^2 = 10$.
(*a*) $t = 0.5$, (*b*) $t = t_s = 0.6192$.

figure 3*a*) except that the high-temperature plume is located farther upstream, and the temperature gradients on the upstream side of the expanding plume are larger. The heated plume tends to be convected upstream by the buoyancy force acting in the negative x-direction, accelerating the 'ploughing' motion on the upstream side of the secondary eddy. This results in the onset of the singularity at a much earlier time, i.e. $t_s = 0.6192$, than for the forced-convective case ($t_s = 1.0127$). Observe also that in the forced-convective case a portion of the secondary eddy is entrained within the erupting spire (see figure 3*b*); whereas, for the case shown in figures 7 and 8, the singularity occurs slightly upstream of the secondary eddy which appears largely unaffected by the onset of the singularity.

For an inclination angle of $\theta = 90°$, where the buoyancy force acts in the down-

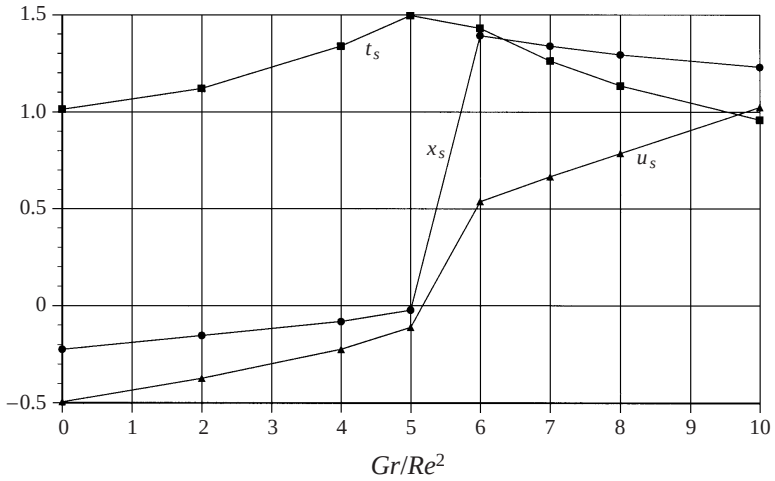

FIGURE 9. Singularity time t_s, position x_s and speed u_s for $\theta = 90°$ and various Gr/Re^2.

stream, i.e. positive x, direction, the results are qualitatively different. Figure 9 shows the singularity time, position and speed as Gr/Re^2 is increased. The results for cases with $Gr/Re^2 \geqslant 6$ have been computed on a 401×201 grid with $a = b = 2$. For $Gr/Re^2 \leqslant 5$ the trends indicated above for $0° < \theta < 180°$ continue, namely that the singularity is delayed as Gr/Re^2 is increased. This is a result of the buoyancy force acting on the high-temperature plume, counteracting the upstream motion of the growing spike. The streamline pattern shown in figure 10(*a*) is indicative of the flow at early times in this regime in that the secondary eddy appears closer to the surface than for the forced-convective case but at approximately the same time, and it grows less rapidly. Observe also that the dividing streamlines between the primary vortex and the surrounding flow bow out near the surface. This type of behaviour is reminiscent of the results for the vortex-induced boundary layer above a moving wall as the wall speed is increased (Doligalski & Walker 1984; Degani *et al.* 1998).

It has been found that between $Gr/Re^2 = 5$ and 6 there is a distinct change in the nature of the flow during the latter stages of the boundary-layer calculation resulting in a significant change in the location and velocity of the singularity as shown in figure 9; in addition, there is a reversal in the trend observed for $Gr/Re^2 \leqslant 5$ in which the singularity time is delayed. The reason for the abrupt change in the singularity is evident in figures 10(*b*) and 11(*b*) which show the instantaneous streamlines and isotherms, respectively, at the singularity time for the case with $Gr/Re^2 = 6$. Although a spike has formed on the upstream side of the secondary eddy as before, its streamwise thickness is significantly greater and it does not result in a singularity. Instead a singularity forms at the streamwise location $x_s = 1.3923$ and is moving downstream with a velocity of $u_s = 0.5444$ rather than moving upstream as in the previous cases described. It is evident from the streamlines and isotherms at the singularity time that the singularity is somewhat weaker in the sense that the gradients are much less severe where the eruption occurs. It appears that the buoyancy force, which acts in the positive x-direction, is large enough both to inhibit the formation of the primary spike on the upstream side of the secondary eddy and to induce a flow on the downstream side of the thermal plume that results in a singularity. Observe from figure 10(*b*) that a recirculation region forms between $x = 2$ and $x = 3$; this recirculation region is present in all cases with $Gr/Re^2 \geqslant 6$ and forms just prior to the onset of the

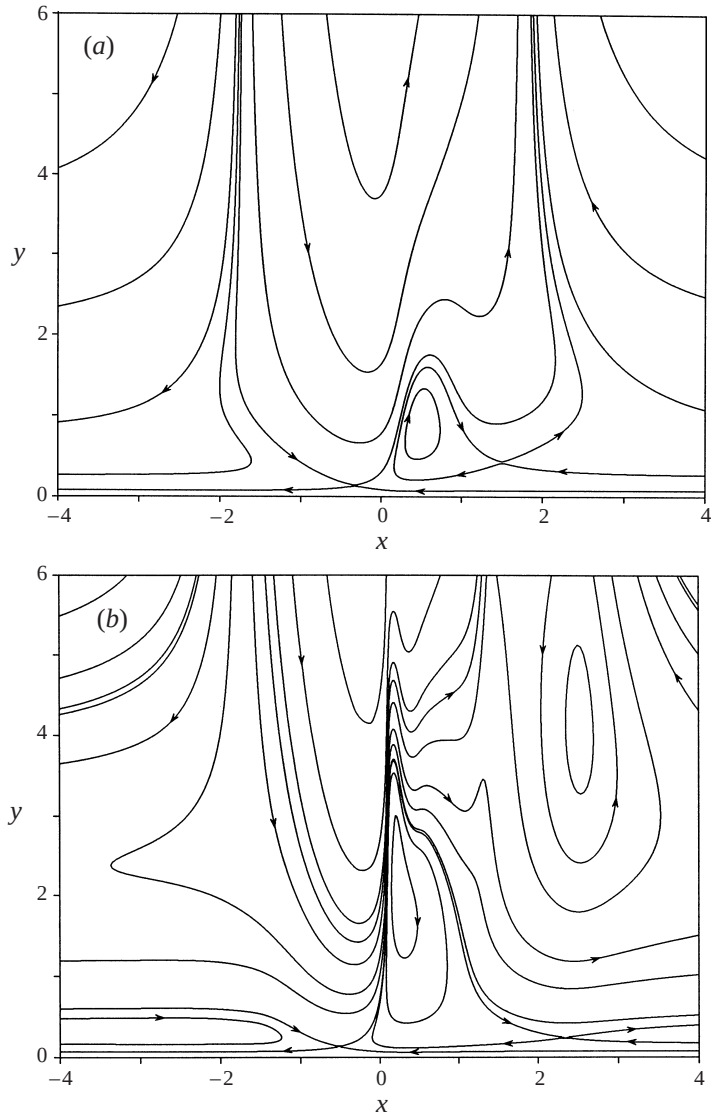

FIGURE 10. Instantaneous streamlines for $\theta = 90°$, $Gr/Re^2 = 6$. (*a*) $t = 0.6$, (*b*) $t = t_s = 1.4298$.

singularity. It is not clear, however, whether this recirculation region plays a role in the formation of the singularity or is a consequence of the events leading up to it. It is interesting to note that there must be a value of Gr/Re^2 between 5 and 6 for which the solution contains both types of singularities occurring simultaneously; no attempt, however, has been made to determine the value for which this occurs.

Similar behaviour is observed as the magnitude of the buoyancy force is increased beyond $Gr/Re^2 = 6$. Figures 12 and 13 show the streamlines and isotherms, respectively, for the case with $\theta = 90°$ and $Gr/Re^2 = 10$. Again the secondary recirculation appears closer to the surface but at approximately the same time as in the forced-convective case. However, in comparing figures 12(*a*) and 12(*b*), it is evident that the secondary eddy remains largely unchanged and is no longer a primary feature of the flow. Instead, the erupting plume of high-temperature fluid is convected downstream

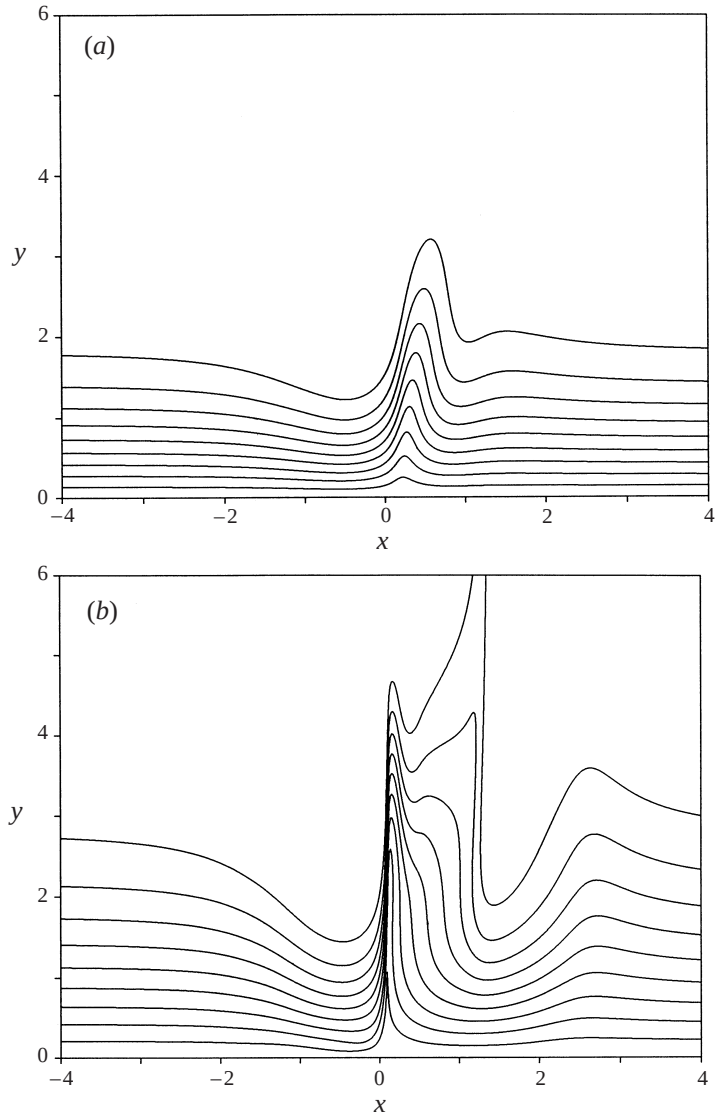

FIGURE 11. Isotherms in increments of $T = 0.1$ for $\theta = 90°$, $Gr/Re^2 = 6$.
(*a*) $t = 0.6$, (*b*) $t = t_s = 1.4298$.

by the buoyancy force, the temperature gradients intensify on the downstream side of the plume, and a singularity occurs at time $t_s = 0.9590$ at $x_s = 1.2294$ and is moving downstream with a velocity of $u_s = 1.0268$. Note that the singularity occurs much sooner than the case with $Gr/Re^2 = 6$, and its streamwise velocity is significantly greater.

4. Discussion

Numerical solutions of the unsteady mixed-convection boundary-layer equations for the flow induced by a rectilinear vortex above an infinite plane surface have been obtained in Lagrangian coordinates. The solutions for various values of the

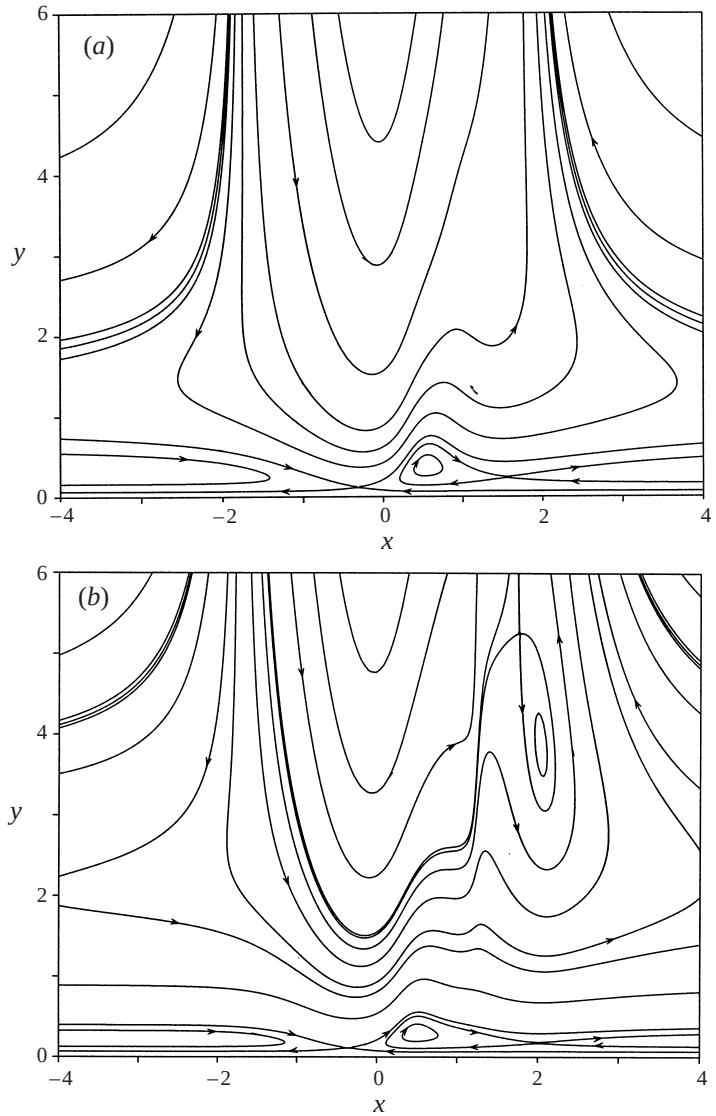

FIGURE 12. Instantaneous streamlines for $\theta = 90°$, $Gr/Re^2 = 10$. (*a*) $t = 0.6$, (*b*) $t = t_s = 0.9594$.

inclination angle and magnitudes of the buoyancy force show that there is a strong coupling between the fluid flow and heat transfer within the boundary layer. The abrupt changes in the flow field as the eruption takes place cause severe gradients in the temperature field and in the convective heat transfer coefficient along the surface. In addition, the erupting boundary layer ejects a spire of high-temperature fluid from adjacent to the surface into the outer flow, significantly enhancing thermal mixing.

The results also show that depending upon the orientation of the surface, buoyancy forces acting on the heated fluid near the surface can alter the flow such that the eruptive process is accelerated or delayed. The strong outflows that develop normal to the surface during the unsteady separation process lead to the formation of a high-temperature plume, and the action of the buoyancy force on this plume modifies the unsteady separation singularity. In the forced-convection case, i.e. $\theta = 0°, 180°$,

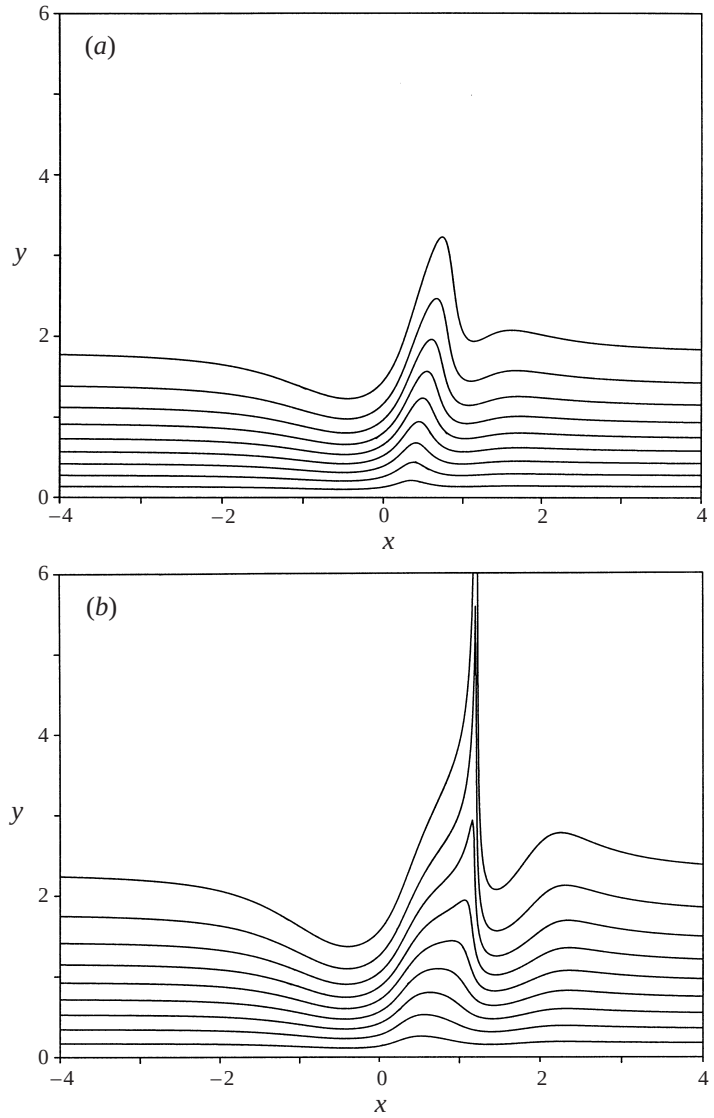

FIGURE 13. Isotherms in increments of $T = 0.1$ for $\theta = 90°$, $Gr/Re^2 = 10$.
(*a*) $t = 0.6$, (*b*) $t = t_s = 0.9594$.

the unsteady eruption and resulting high-temperature plume convect upstream as the singularity is approached. In the mixed-convection case, however, the upstream motion of the erupting spike and corresponding high-temperature plume is either accelerated, decelerated or even reversed by the action of the buoyancy force. When the inclination angle of the surface is such that $0° < \theta < 180°$, the buoyancy force acts in the opposite direction to the local adverse pressure gradient, effectively dampening its effect on the boundary layer and delaying separation for small magnitudes of the buoyancy force. For larger values of Gr/Re^2, the buoyancy force acting on the high-temperature plume is sufficient to reverse its direction and induce a somewhat weaker singularity on the downstream side of the high-temperature plume. When $180° < \theta < 360°$, on the other hand, the buoyancy force acts in the same direction

as the adverse pressure gradient, and the separation process is accelerated. Note that these results have been obtained using the Boussinesq approximation for which $(T_s - T_\infty)/T_\infty \ll 1$; therefore, the strong coupling observed here can be achieved with relatively small differences in temperature between the surface and the ambient flow.

It is of interest to consider how the singular behaviour that occurs in the unsteady mixed-convection boundary-layer results shown here relates to the singular structures observed in similar flows, namely the non-interactive boundary-layer singularity found by Van Dommelen & Shen (1982) and Elliott *et al.* (1983) and its modified form for the case of a moving wall determined by Degani *et al.* (1998). The non-interactive boundary-layer singularity applies to the fluid flow portion of the forced-convective cases in the present investigation. A similarity solution develops for the flow locally surrounding the separation point as the singularity time is approached. This similarity solution, sometimes referred to as the terminal boundary-layer solution, describes a flow structure in which the boundary layer splits into two shear layers that surround an intermediate region in which the velocity is nearly constant. The upper shear layer moves away from the surface at a rate proportional to $(t_s - t)^{-1/4}$, where t_s is the non-interactive singularity time.

The influence of a moving wall on the non-interactive boundary-layer singularity has been investigated by Degani *et al.* (1998). They have found that as the speed of the wall is increased in the same direction as the local mainstream flow, unsteady separation can be suppressed due to the elimination of the upper shear layer. The strength of the upper shear layer is given by $U_\infty(x_s) - u_s$, where $U_\infty(x_s)$ is the local mainstream velocity (see equation (2.1)) at the streamwise location of the singularity, and u_s is the speed of the separation point at the time the singularity occurs. Suppression of the unsteady separation singularity for the case of a moving wall occurs when $U_\infty(x_s) - u_s \to 0$. In order to determine whether unsteady separation is suppressed by a similar mechanism in the unsteady mixed-convection boundary layer considered here, the data in figure 9 for $\theta = 90^\circ$ is used to determine whether $U_\infty(x_s) - u_s$ vanishes with increasing buoyancy force. Recall that for this case, the singularity time is delayed on increasing Gr/Re^2 up to some value of the buoyancy force in the range $5 < Gr/Re^2 < 6$ at which the singularity is suppressed, and above which the flow evolves rather differently, terminating in a singularity that is somewhat weaker and occurs at a different location. As shown in table 1, $U_\infty(x_s) - u_s$ experiences an abrupt step change between $5 < Gr/Re^2 < 6$ when the primary singularity is suppressed, rather than a gradual approach to zero as in the case of a moving wall. Therefore, suppression of unsteady separation is apparently by a different mechanism for the mixed-convection boundary layer than for the case with a moving wall, as the strength of the upper shear layer does not weaken significantly prior to suppression of separation.

Returning to the issue of the structure of the singularity that occurs in the unsteady mixed-convection boundary-layer equations, this structure apparently is significantly more complex than that found by Van Dommelen & Shen (1982) and Elliott *et al.* (1983) for the non-interactive boundary-layer singularity. It must have as a special case the non-interactive boundary-layer singularity, i.e. for forced-convection flow, but must also encompass the coupled effects of the momentum and thermal boundary layers and the weaker singularity that occurs, for example, when $\theta = 90^\circ$ and $Gr/Re^2 > 5$. This latter singularity probably has a structure that is significantly different from that for the forced-convective case.

The unsteady mixed-convection boundary-layer results shown here suggest that it may be possible to use local heating (or cooling) of the surface to control the

Gr/Re^2	t_s	x_s	u_s	$U_\infty(x_s) - u_s$
0.0	1.0127	−0.2243	−0.4951	3.3035
2.0	1.1200	−0.1532	−0.3729	3.2812
4.0	1.3373	−0.0818	−0.2235	3.1969
5.0	1.4954	−0.0233	−0.1109	3.1088
6.0	1.4298	1.3920	0.5368	−0.1831
7.0	1.2607	1.3379	0.6665	−0.2328
8.0	1.1335	1.2927	0.7870	−0.2894
10.0	0.9594	1.2293	1.0244	−0.4341

TABLE 1. Variation of t_s, x_s, u_s and $U_\infty(x_s) - u_s$ with Gr/Re^2 for the case with $\theta = 90°$.

unsteady separation process in certain applications. Other methods of control, such as suction (Karim & Acharya 1994; Alrefai & Acharya 1996) or a moving wall (Degani *et al.* 1998) are potentially well suited to situations in which the location of unsteady separation is known *a priori* and changes little for various flow conditions. This is true, for example, in the case of leading-edge separation on airfoils (Karim & Acharya 1994; Degani, Li & Walker 1996). In many cases, however, the location of unsteady separation can vary significantly with flow conditions; therefore, these fixed methods of control would be difficult to implement. This is true, for example, in the vortex-induced eruption that occurs on the upper surface of a pitching airfoil and causes detachment of the dynamic stall vortex. In such situations it may be possible to control unsteady separation using a locally heated (or cooled) surface. Some means of sensing where and when unsteady separation will occur would be necessary, and then the local region determined to have optimum influence upon the separation process could be heated (or cooled) at the appropriate time during the evolution of the flow. The resulting buoyancy forces could then be used to accelerate, delay or alter the nature of the unsteady separation depending on the orientation of the surface and the magnitude of the buoyancy force. For example, when the buoyancy force acts in the opposite direction to the adverse pressure gradient, the singularity is delayed for small Gr/Re^2. For larger magnitudes of the buoyancy force, the primary singularity can be suppressed and a somewhat weaker secondary singularity induced at a different location.

This work was supported by the National Research Council Postdoctoral Fellowship Program and the US Army Research Office under grant number DAAG55-98-1-0384. The author would like to thank the referees for a number of insightful comments.

REFERENCES

ADAMS, E. C., CONLISK, A. T. & SMITH, F. T. 1995 Adaptive grid scheme for vortex-induced boundary layers. *AIAA J.* **33**, 864–870.

ALREFAI, M. & ACHARYA, M. 1996 Controlled leading-edge suction for management of unsteady separation over pitching airfoils. *AIAA J.* **34**, 2327–2336.

BUCKMASTER, J. 1970 The behaviour of a laminar compressible boundary layer on a cold wall near a point of zero skin friction. *J. Fluid Mech.* **44**, 237–247.

CASSEL, K. W. 1996 A numerical evaluation of the theoretical description of unsteady separation. *AIAA Paper* 96-2143.

CASSEL, K. W. 2000 A comparison of Navier–Stokes solutions with the theoretical description of unsteady separation. *Phil. Trans. R. Soc. Lond.* A **358**, 3207–3227.

Cassel, K. W., Smith, F. T. & Walker, J. D. A. 1996 The onset of instability in unsteady boundary-layer separation. *J. Fluid Mech.* **315**, 223–256.

Chandrasekhara, M. S., Wilder, M. C. & Carr, L. W. 1997 Control of flow separation using adaptive airfoils. *AIAA Paper* 97-0655.

Daniels, P. G. 1992 A singularity in thermal boundary-layer flow on a horizontal surface. *J. Fluid Mech.* **242**, 419–440.

Daniels, P. G. & Gargaro, R. J. 1993 Buoyancy effects in stably stratified horizontal boundary-layer flow. *J. Fluid Mech.* **250**, 233–251.

Davies, T. & Walker, G. 1977 On solutions of the compressible laminar boundary-layer equations and their behaviour near separation. *J. Fluid Mech.* **80**, 279–292.

Degani, A. T., Li, Q. & Walker, J. D. A. 1996 Unsteady separation from the leading edge of a thin airfoil. *Phys. Fluids* **8**, 704–714.

Degani, A. T., Walker, J. D. A. & Smith, F. T. 1998 Unsteady separation past moving surfaces. *J. Fluid Mech.* **375**, 1–38.

Doligalski, T. L., Smith, C. R. & Walker, J. D. A. 1994 Vortex interactions with walls. *Ann. Rev. Fluid Mech.* **26**, 573–616.

Doligalski, T. L. & Walker, J. D. A. 1984 The boundary layer induced by a convected two-dimensional vortex. *J. Fluid Mech.* **139**, 1–28.

Elliott, J. W., Cowley, S. J. & Smith, F. T. 1983 Breakdown of boundary layers: (i) on moving surfaces; (ii) in semi-similar unsteady flow; (iii) in fully unsteady flow. *Geophys. Astrophys. Fluid Dyn.* **25**, 77–138.

Goldstein, S. 1948 On laminar boundary-layer flow near a point of separation. *Q. J. Mech. Appl Maths* **1**, 43–69.

Higuera, F. J. 1997 Boundary layer separation due to gas thermal expansion. *Phys. Fluids* **9**, 2841–2850.

Hoyle, J. M., Smith, F. T. & Walker, J. D. A. 1991 On sublayer eruption and vortex formation. *Comput. Phys. Commun.* **65**, 151–157.

Hunt, R. & Wilks, G. 1980 On the behaviour of the laminar boundary-layer equations of mixed convection near a point of zero skin friction. *J. Fluid Mech.* **101**, 377–391.

Karim, M. A. & Acharya, M. 1994 Suppression of dynamic-stall vortices over pitching airfoils by leading-edge suction. *AIAA J.* **32**, 1647–1655.

Kiran, A. S., Varley, E. & Walker, J. D. A. 1996 Unsteady motion induced on a flexible surface in a high Reynolds number flow. *AIAA Paper* 96-2138.

Li, L., Walker, J. D. A., Bowles, R. I. & Smith, F. T. 1998 Short-scale break-up in unsteady interactive layers: local development of normal pressure gradients and vortex wind-up. *J. Fluid Mech.* **374**, 335–378.

Merkin, J. H. 1969 The effect of buoyancy forces on the boundary-layer flow over a semi-infinite vertical flat plate in a uniform free stream. *J. Fluid Mech.* **35**, 439–450.

Modi, V. J., Munshi, S. R. & Bandyopadhyay, G. 1998 High-performance airfoil with moving surface boundary-layer control. *J. Aircraft* **35**, 544–553.

Pal, D. & Sinha, S. 1998 Controlling unsteady separation on a cylinder with a driven flexible wall. *AIAA J.* **36**, 1023–1028.

Peridier, V. J., Smith, F. T. & Walker, J. D. A. 1991*a* Vortex-induced boundary-layer separation. Part 1. The unsteady limit problem $Re \rightarrow \infty$. *J. Fluid Mech.* **232**, 99–131.

Peridier, V. J., Smith, F. T. & Walker, J. D. A. 1991*b* Vortex-induced boundary-layer separation. Part 2. Unsteady interacting boundary-layer theory. *J. Fluid Mech.* **232**, 133–165.

Puhak, R. I., Degani, A. T. & Walker, J. D. A. 1995 Unsteady separation and heat transfer upstream of obstacles. *J. Fluid Mech.* **305**, 1–27.

Rehm, R. G., Cassel, K. W., McGrattan, K. B. & Baum, H. R. 1995 Gravity-current transport in building fires. *Proc. 8th Intl Symp. on Transport Phenomena in Combustion* (ed. S. H. Chan), Vol. 1, pp. 745–756. Taylor & Francis.

Schneider, W. & Wasel, M. G. 1985 Breakdown of the boundary-layer approximation for mixed convection above a horizontal plate. *Intl J. Heat Mass Transfer* **28**, 2307–2313.

Smith, F. T. 1988 Finite-time break-up can occur in any unsteady interacting boundary layer. *Mathematika* **35**, 256–273.

Stewartson, K. 1962 The behaviour of a laminar compressible boundary layer near a point of zero skin-friction. *J. Fluid Mech.* **12**, 117–128.

Van Dommelen, L. L. & Shen, S. F. 1982 The genesis of separation. *Numerical and Physical Aspects of Aerodynamic Flows* (ed. T. Cebeci), pp. 293–311. Springer.

Walker, J. D. A. 1978 The boundary layer due to a rectilinear vortex. *Proc. R. Soc. Lond.* A **359**, 167–188.

Wickern, G. 1991*a* Mixed convection from an arbitrarily inclined semi-infinite flat plate. Part 1. The influence of the inclination angle. *Intl J. Heat Mass Transfer* **34**, 1935–1945.

Wickern, G. 1991*b* Mixed convection from an arbitrarily inclined semi-infinite flat plate. Part 2. The influence of the Prandtl number. *Intl J. Heat Mass Transfer* **34**, 1947–1957.

Wilks, G. 1974 A separated flow in mixed convection. *J. Fluid Mech.* **62**, 359–368.

Xiao, Z., Adams, E. C. & Conlisk, A. T. 1996 Terminal structure of unsteady classical and interacting boundary layers. *Phys. Fluids* **8**, 1397–1407.